International Journal of Hydrogen Energy 106 (2025) 973–979

Contents lists available at ScienceDirect

International Journal of Hydrogen Energy

journal homepage: www.elsevier.com/locate/he

Rapid synthesis of phase-engineered tungsten carbide electrocatalysts via flash joule heating for high-current-density hydrogen evolution

Amirarsalan Mashhadian [a], Shiwen Wu [a], Taesoon Hwang [b], Yun Hao [a], Mahdi Mosadegh [a], Kyeongjae Cho [b], Dewen Hou [c], Tianyi Li [d], Majid Minary-Jolandan [a,**], Guoping Xiong [a,*]

[a] Department of Mechanical Engineering, The University of Texas at Dallas, 800 W Campbell Rd, Richardson, TX, 75080, United States
[b] Department of Material Science Engineering, The University of Texas at Dallas, 800 W Campbell Rd, Richardson, TX, 75080, United States
[c] Center for Nanoscale Materials, Argonne National Laboratory, 9700 South Cass Avenue, Lemont, IL, 60439, United States
[d] X-ray Science Division, Argonne National Laboratory, 9700 South Cass Avenue, Lemont, IL, 60439, United States

ARTICLE INFO

Handling Editor: Jinlong Gong

Keywords:
Acidic hydrogen evolution reaction
Tungsten carbides
Flash joule heating
Phase engineering

ABSTRACT

Fabricating durable and high-performance electrocatalysts operating at high current densities for industrial acidic hydrogen evolution remains a daunting challenge. Tailoring the phase composition of electrocatalysts is a promising strategy to harness synergistic effects and improve charge transfer, thereby optimizing their performance. This work presents a fast, green method based on flash joule heating (FJH) to synthesize phase-engineered tungsten carbide electrocatalysts for the acidic hydrogen evolution reaction (HER) at high current densities. Tungsten carbide electrodes with varying FJH treatment durations (3, 10, 30, and 60 s) are fabricated to fine-tune the mixture of tungsten monocarbide (WC) and tungsten semicarbide (W_2C) phases. Results show that samples with a 30-s treatment (TC-3) exhibit an optimal balance between these phases, leading to a low overpotential of 180.97 and 387 mV at current densities of 10 mA/cm^2 and 4 A/cm^2, respectively. TC-3 exhibits significantly lower charge transfer resistance compared to the other electrocatalysts, which can be attributed to its optimal phase ratio. Notably, the TC-3 electrocatalyst remains stable for over 9 days at 4 A/cm^2 due to their controlled phases and excellent corrosion-resistant properties. This work highlights a new method to fabricate cost-effective, high-performance tungsten carbide electrocatalysts with well-controlled phase compositions.

1. Introduction

The excessive reliance on fossil fuels has led to severe environmental pollution and global warming, creating an urgent need for renewable and clean energy sources as alternatives [1–3]. Hydrogen has emerged as a promising energy carrier for meeting clean energy demands due to its high energy density and environmentally benign properties [4–7]. Electrocatalytic hydrogen production offers an economical and efficient approach to achieving a closed carbon cycle [8–12]. Currently, platinum (Pt) stands as the most efficient electrocatalyst for the hydrogen evolution reaction (HER) in acidic media due to its favorable electronic structure, which facilitates moderate binding energy with hydrogen ions [13], a crucial attribute for achieving efficient catalytic performance [14,15]. The Pt catalysts for the HER in acidic media suffer from two major limitations including their high cost [16], which hinders large-scale production [17], and performance deterioration at high current densities due to catalyst restructuring issues [18,19].

Transition metal (e.g., Mo, W) carbides (TMCs) have been considered as promising alternatives to Pt catalysts for HER due to their low cost and Pt-like electronic structures [20–22]. Particularly, tungsten carbide shows exceptional performance (e.g., low overpotential and long-term stability) at high current densities stemming from its corrosion resistance nature and high electronic conductivity [23]. Tungsten carbide possesses multiple phases, such as tungsten monocarbide (WC) and tungsten semi-carbide (W_2C), exhibiting diverse electrocatalytic properties for HER [24]. The synergetic effects of these phases can lead to improved HER activity by modulating the hydrogen adsorption energy due to different interactions and charge transfer mechanisms at the phase interfaces [25,26]. Despite recent studies on molybdenum carbide phase optimization in alkaline media [27], no solid work has been reported on optimizing tungsten carbide phases for hydrogen evolution reaction (HER) at high current densities (>3 A/cm^2) in acidic media

* Corresponding author.
** Corresponding author.
E-mail addresses: Majid.Minary@utdallas.edu (M. Minary-Jolandan), Guoping.Xiong@utdallas.edu (G. Xiong).

https://doi.org/10.1016/j.ijhydene.2025.01.487
Received 29 September 2024; Received in revised form 23 January 2025; Accepted 31 January 2025
Available online 8 February 2025

[28]. Thus, optimizing the composition of different tungsten carbide phases is crucial to improving the HER activity of the catalyst.

In this study, a rapid, cost-effective, and environment-friendly method based on flash Joule heating (FJH) has been implemented to fabricate tungsten carbide catalysts with optimized phases, as efficient alternatives to Pt, for high-performance acidic hydrogen production at industrial-level current densities. A series of tungsten carbide electrodes were synthesized with different FJH durations (3, 10, 30, and 60 s) at 900 °C to tailor the phase composition of WC and W_2C. The results revealed that the sample synthesized for 30 s (denoted as TC-3) exhibited the optimal performance at low current density and especially high current density of 4 A/cm^2, attributed to the optimized ratio of WC to W_2C phases and consequent faster electron transfer. Remarkably, the TC-3 sample demonstrated exceptional stability, maintaining its performance for over 9 days of continuous operation at 4 A/cm^2, ascribed to the inherent corrosion-resistant properties of tungsten carbide and strong tungsten-carbon bonding. This work paves the way for the scalable production of cost-effective and robust tungsten carbide catalysts outperforming Pt, particularly for high-current-density industrial hydrogen production applications where high throughput and long-term stability are crucial.

2. Experimental section

2.1. Preparation of the tungsten carbide electrode

Carbon papers (MGL 190, Fuel Cell Earth Co.) were cleaned in a sonication process using acetone (Sigma Aldrich), followed by 2-propanol (Fisher Scientific Co.), and then deionized (DI) water. Subsequently, the surface of carbon papers was treated by air plasma (Harrick Plasma) at a medium intensity of 10.5 W for 1 min to become hydrophilic. A 0.5 M sodium tungstate (Na_2WO_4, STREM Co.) solution was prepared by dissolving 1649.3 mg of the salt precursor in 10-mL DI water with the assistance of sonication for 15 min (Fig. 1a). Carbon paper substrates (8mm × 20 mm) were immersed in the prepared solution for 20 min and then dried for 30 min at 60 °C in an oven. To synthesize tungsten carbides, the prepared samples were sandwiched between two pieces of graphite felts, and the temperature was ramped up to 900 °C by FJH within 1 s (Fig. 1b and c). Tungsten carbides were synthesized for durations of 3, 10, 30, and 60 s, corresponding to samples denoted as TC-1, TC-2, TC-3, and TC-4, respectively. Following the fabrication of tungsten carbide on carbon paper substrates, the samples were washed multiple times with ethanol and DI water to remove any salt residues. To prepare the commercial Pt/C powder catalysts, 2 mg of catalyst was uniformly dispersed in 1.0 mL of absolute ethanol along with 40 μL of a 5.0 wt% Nafion solution to create a homogeneous catalyst ink (2 mg mL^{-1}) through a 1-h sonication process. Subsequently, 250 μL of the ink was deposited onto the surface of a carbon paper substrate (4 cm × 1 cm) and dried overnight.

2.2. Characterization

The phase composition of the samples was analyzed by X-ray diffraction within the range from 30° to 70° (XRD, Bruker D8 P-XRD) using Cu Kα radiation (λ = 1.5418 Å). The morphology of as-prepared tungsten carbides was studied by scanning electron microscopy (SEM, Zeiss Supra 40) and transmission electron microscopy (TEM, 200 kV, JEOL 2100). The chemical analysis of the samples was conducted by high-resolution X-ray photoelectron spectroscopy (XPS, Versa probe II). The pass energy and energy step size for XPS were chosen to be 50 eV and 0.1 eV, respectively. Raman spectra were collected using Horiba Raman microscope with an excitation laser of 532 nm at a magnification of 50×.

2.3. Electrochemical measurements

A three-electrode configuration was used for the electrochemical measurement in 0.5 M H_2SO_4 aqueous electrolyte solution (pH ≈ 0.3). In the electrochemical tests, voltage and current were controlled and measured by a potentiostat (Gamry interface 1010E). A graphite rod and an Ag/AgCl electrode were employed as counter and reference electrodes, respectively. The activation of tungsten carbide electrodes was implemented by performing cyclic voltammetry (CV) for 50 cycles. Linear scan voltammetry (LSV) was carried out with a scan rate of 2 mV/s. The stability tests were conducted by using chronopotentiometry techniques at a given constant voltage in the H-cell setup similar to the

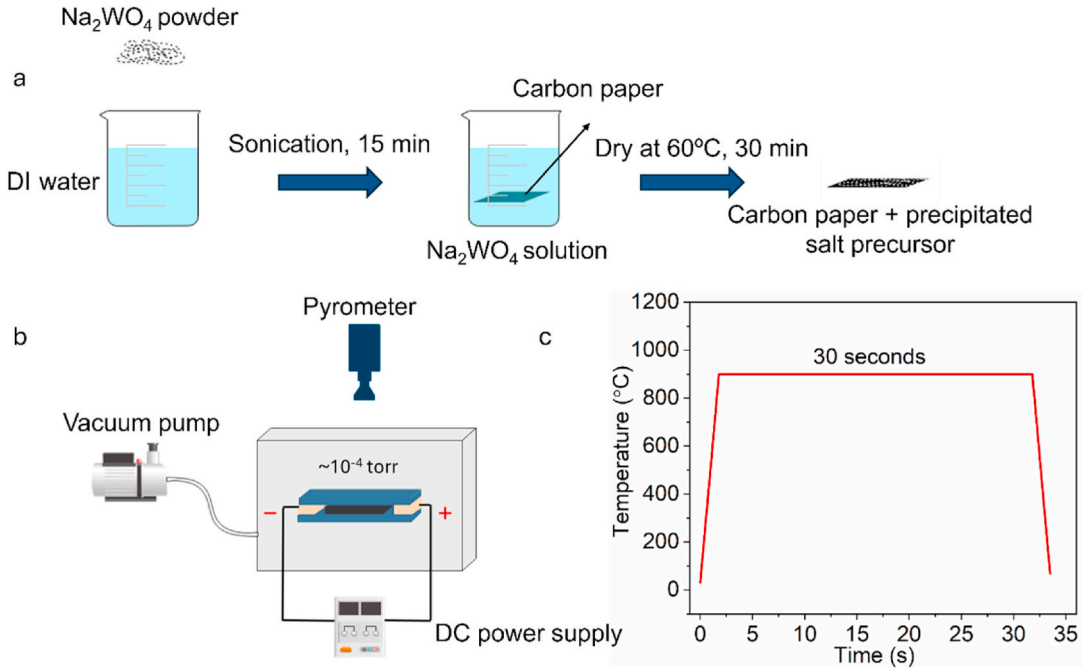

Fig. 1. (a) Schematic of the fabrication process of tungsten carbide electrocatalyst using a carbon paper substrate. (b) Schematic of the FJH experimental setup to fabricate tungsten carbide electrocatalyst. (c) Temperature-time curves during the FJH process.

references for large current densities [29]. Potentiostatic electrochemical impedance spectroscopy (EIS) was performed over a frequency range from 100 kHz to 0.01 Hz at a specific applied potential. Additionally, cyclic voltammetry was conducted within the non-faradaic potential window (0.2–0.3 V vs. RHE) to calculate the electric double-layer capacitance. The electrochemical active surface area (ECSA) was calculated using the ratio of the double-layer capacitance to the specific capacitance, which is approximately 40 μF/cm^2.

All of the potential values are reported after *iR* compensation and versus reversible hydrogen electrode (RHE), which were calculated using the following equation [30]: $E_{RHE} = E_{Ag/AgCl} + E^{\circ}_{Ag/AgCl} + (0.059 \times pH)$. In the above equation, E_{RHE} represents the calculated potential versus the RHE, $E_{Ag/AgCl}$ denotes the measured potential relative to the Ag/AgCl reference electrode, and $E^{\circ}_{Ag/AgCl}$ is the standard electrode potential (E° = 0.197 V at 25 °C) for the Ag/AgCl electrode.

2.4. DFT calculation

The atomic and electronic structures were examined by density functional theory (DFT) calculations. All DFT calculations were conducted by using the Vienna Ab Initio Simulation Package (VASP) implementing the exchange-correlation functional of the spin-polarized generalized gradient approximation (GGA) parameterized by Perdew-Burke-Ernzerhof (PBE) of W and C [31]. Structures of bulk WC, W_2C, and WC-W_2C interface were simulated based on Gamma-centered grid of 9 × 9 × 9, 5 × 4 × 4 and 1 × 4 × 4 k-point grids with a cut-off energy of 500 eV, respectively. All the structures were fully relaxed for thermodynamic stabilization. The d-band center (d_{center}) was conducted following:

$$d_{center} = \frac{\int EPDOS(E)dE}{\int PDOS(E)dE} \quad (1)$$

3. Results and discussion

The XRD patterns of the samples prepared by different FJH durations (i.e., TC-1, TC-2, TC-3, and TC-4) are shown in Fig. 2a and coincide with those reported in prior work [32], confirming the successful synthesis of tungsten carbides in all these samples. Moreover, varying the FJH duration effectively influences the phase compositions such as tungsten (W), WC, and W_2C phases in the products and their relative quantities. As shown in Fig. 2a, TC-1 exhibits characteristic peaks located at 34.6°, 38.1°, and 39.5° corresponding to the hexagonal W_2C phase [33], while TC-2, TC-3, and TC-4 display characteristic peaks for both hexagonal WC (JCPDS No. 51–0939) and W_2C (JCPDS No. 35–0776) phases. The maximum ratio intensities of WC:W_2C:W are 0:0.41:0.59, 0.42:0.50:0.08, 0.19:0.68:0.13, and 0.48:0.40:0.12 for samples TC-1, TC-2, TC-3, and TC-4, respectively, indicating that the duration of FJH treatment can effectively modulate the ratio between the various tungsten carbide phases. We believe that the carbon source for the synthesis of tungsten carbides originate from the carbon fiber substrate itself, a similar phenomenon observed in the prior work [34].

Raman spectroscopy provides additional information about the structures of FJH-synthesized samples. For TC-1, a characteristic peak is observed at around 686 cm^{-1}, corresponding to the W–C stretching mode. However, this peak becomes broader and weaker for TC-2, TC-3, and TC-4, as the phase-pure WC emerges [35]. The peak located at approximately 250 cm^{-1} is ascribed to oxygen bonding (i.e., WC-O), which is due to the mild oxidation of the sample surface in air. Furthermore, three main characteristic peaks are observed in all the samples at approximately 1340, 1594, and 2700 cm^{-1}, attributed to the D-band (diamond-like carbon), G-band (graphitic carbon), and 2D-band (layered structure of graphite or graphene), respectively (Fig. S1) [36]. The relative intensity ratio of the G-band to D-band, indicative of the graphitic degree of the carbon content, exhibits a direct relationship with the FJH synthesis duration of tungsten carbides, suggesting a more well-defined crystalline structure with increasing FJH durations [8,37].

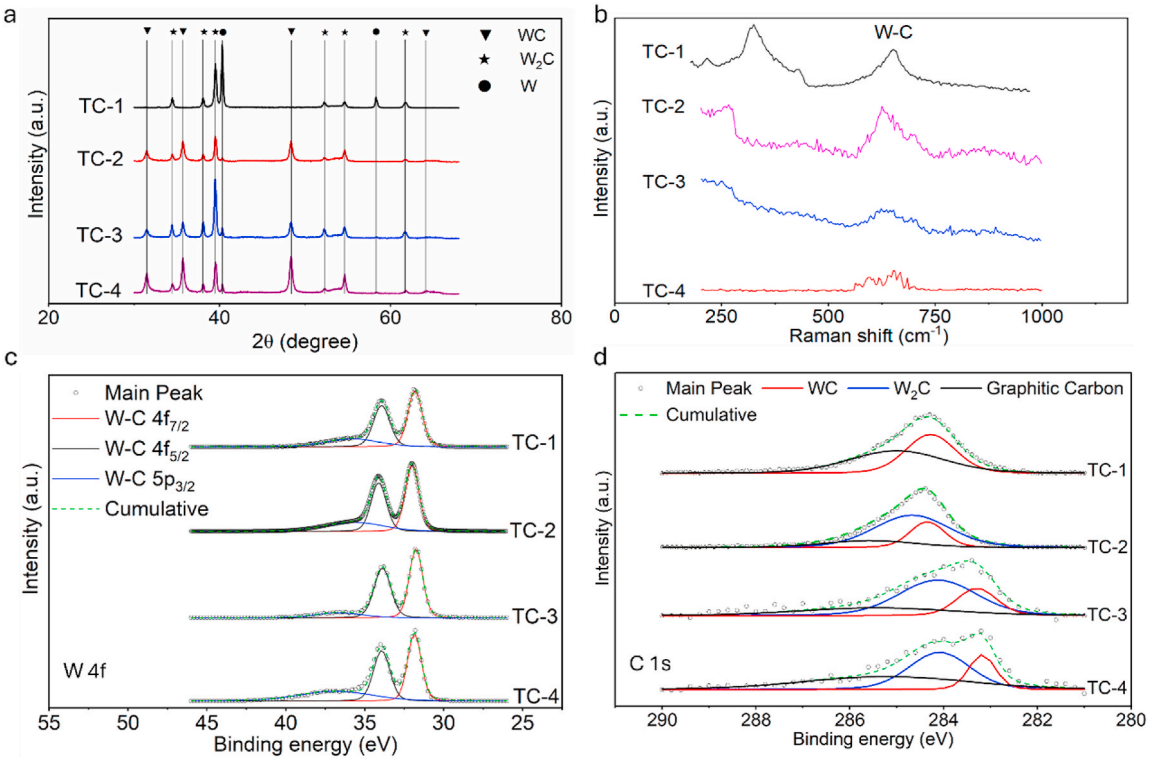

Fig. 2. (a) XRD patterns and (b) Raman spectra of tungsten carbide electrocatalysts with different FJH durations. High-resolution XPS spectra of tungsten carbide electrocatalysts with different FJH durations (c) W 4f, (d) C 1s.

The W–C bonding is confirmed by XPS data, as shown in Fig. 2c. No oxygen bonding to tungsten or carbon is observed, ruling out the possibility of the formation of tungsten oxides (Figs. S2–S5). The absence of oxygen bonding in XPS spectra can be attributed to the removal of the mild surface oxidation layer by sputtering during the test. XPS analysis of the W 4f region reveals binding energies between 31.8 and 32.0 eV, with TC-3 showing the lowest value of 31.8 eV, indicating a more metallic characteristic (or feature) and increased electron density around the tungsten atoms. This higher electron density weakens the interactions between tungsten and hydrogen ions, promoting easier hydrogen desorption, which is critical for efficient HER. Thus, the optimal WC:W_2C ratio in TC-3 enhances electron transfer and reduces tungsten-hydrogen binding energy, leading to improved HER performance. The high-resolution XPS spectra of carbon (Fig. 2d) show no detectable peaks of carbon-oxygen bonding and confirm the presence of WC, W_2C, and graphitic carbon, indicating a pure carbide and graphitic environment.

The microstructural morphology of the synthesized tungsten carbide samples by FJH was investigated by SEM. Specifically, TC-1 exhibits the uniform formation of sparely distributed nanoparticles with sizes ranging from 30 to 50 nm (Fig. 3a and b). For TC-2, densely connected nanoparticles ranging from 50 to 260 nm in size cover the entire carbon fiber surface forming a porous-like structure (Fig. 3c and d). Moreover, a porous structure comprised of uniform, well dispersed nanoparticles with an average size of approximately 70 nm forms on the surface of the TC-3 catalyst (Fig. 3e and f), resulting in more active sites for the HER compared to the other catalysts. In addition, the element distribution of tungsten is uniform throughout the catalysts, suggesting well-dispersed active sites for effective HER (Fig. S6). As shown in Fig. 3g and h, a dense layer is formed on the surface of carbon fiber, indicating the tungsten carbide particles are sintered to be interconnected, which can hinder effective HER in TC-4 electrocatalyst.

High-resolution TEM analysis was conducted to further investigate the atomic structure of the TC-3 electrocatalyst. Fig. 3i reveals the presence of two distinct tungsten carbide phases, WC and W_2C, corroborating the XRD data (Fig. 2a). The observed interlayer distances of 0.279 nm and 0.305 nm correspond to the (100) lattice spacing of W_2C and the (001) lattice spacing of WC, respectively. Fig. 3j highlights the existence of abundant structural defects, including atomic vacancies (indicated by dashed circles) and lattice distortions (indicated by dashed squares). These defects are likely induced by the rapid heating and cooling rates during FJH processes and are known to enhance HER performance [25]. Additionally, Fig. S7 shows two distinct lattice fringes belonging to WC and W_2C, where the phase interface is observed to be continuously reoriented across the boundary. This interaction between the WC and W_2C phases may enhance structural stability, allowing the material to endure harsh electrochemical conditions (e.g., high current densities).

The HER performance of the synthesized tungsten carbide samples with different FJH durations was evaluated in an acidic environment using LSV. Fig. 4a depicts the polarization curves obtained in 0.5 M H_2SO_4 for all fabricated tungsten carbide samples and a commercial Pt/C catalyst. The overpotential of TC-3 at a current density of 10 mA/cm^2 was determined to be 180.97 mV, which is the lowest among the tungsten carbide samples but higher than that (44.19 mV) of Pt/C. The overpotentials (j = 10 mA/cm^2) of TC-1, TC-2, and TC-4 catalysts were 239.02 mV, 194.98 mV, and 187.57 mV, respectively, indicating a dependency of the overpotential on the phase composition of the electrocatalysts. This trend may be attributed to the co-existence of three active components (W, WC, and W_2C) and their potential synergistic effects, resulting in modulated hydrogen binding energy and enhanced charge transfer kinetics [38]. At a high current density of 4 A/cm^2, TC-3 exhibited the best performance (η = 387 mV) among the fabricated tungsten carbide samples, significantly outperforming TC-1 (469.73 mV) and TC-4 (418.39 mV). Remarkably, TC-3 also outperformed Pt/C at current densities exceeding 630 mA/cm^2, demonstrating its exceptional kinetics at high current densities. The superior hydrogen evolution performance of TC-3 suggests the importance of the synergetic

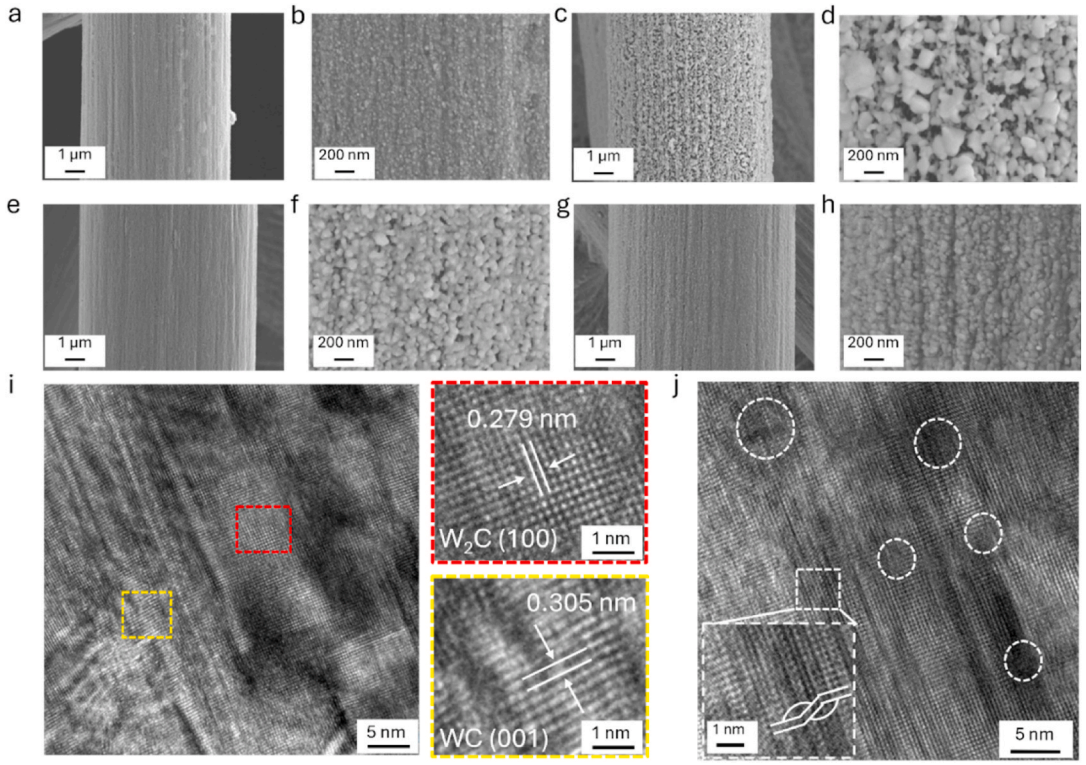

Fig. 3. SEM images of tungsten carbide electrocatalysts with different FJH durations: (a, b) TC-1 (3 s), (c, d) TC-2 (10 s), (e, f) TC-3 (30 s), (g, h) TC-4 (60 s). (i) High-resolution TEM image of TC-3 electrocatalyst. (j) TEM image of TC-3 electrocatalyst with defects including atom vacancy and lattice distortion.

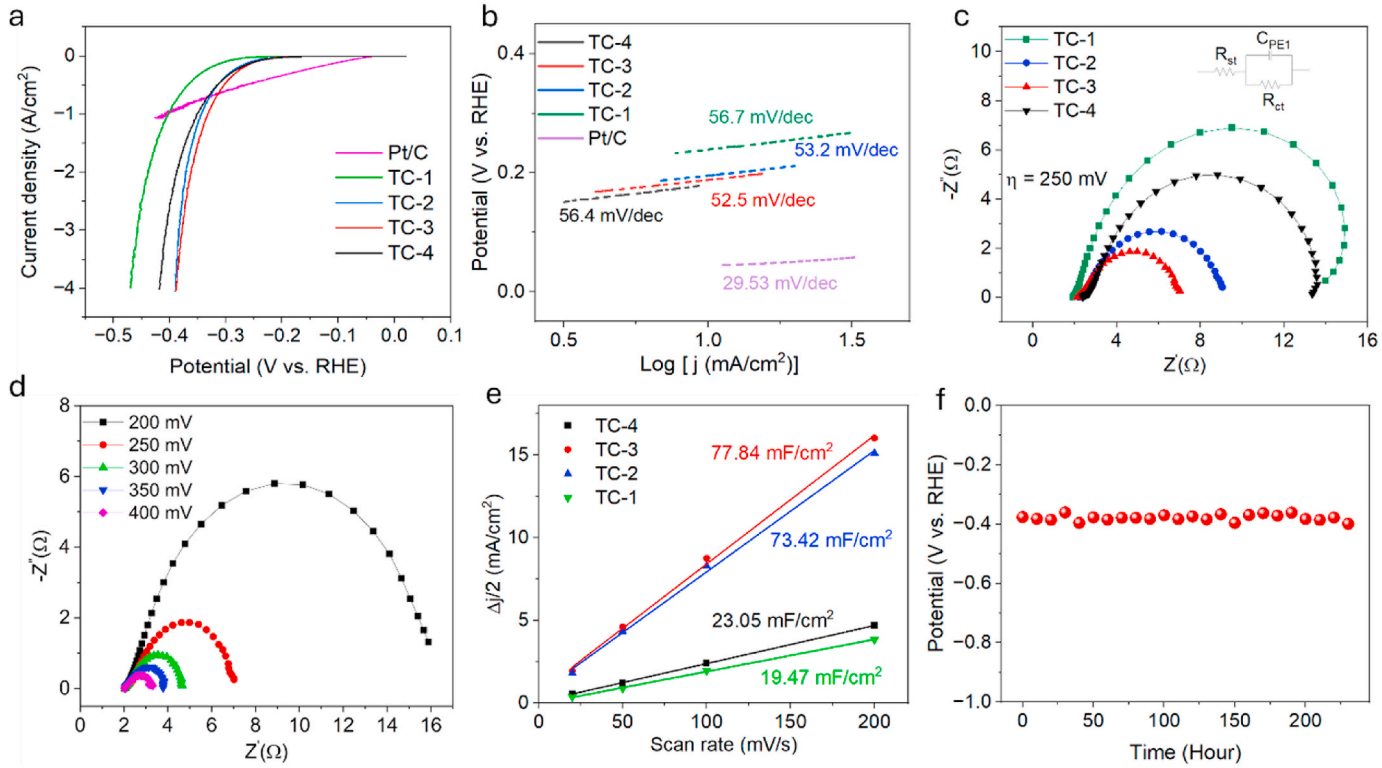

Fig. 4. Comparative performance of Pt/C electrocatalyst and tungsten carbide electrocatalysts with different FJH durations: (a) polarization curves, (b) Tafel curves. (c) Nyquist plot of tungsten carbide electrocatalysts at η = 250 mV. (d) Nyquist plot for the TC-3 at different overpotentials. (e) Capacitive current density as a function of scan rate for different tungsten carbide electrocatalysts. (f) Long-term stability test for TC-3 electrocatalyst at 4 A/cm^2 with iR compensation.

effect between the two phases (i.e., W_2C and WC) and especially their improved interface charge transfer.

The Tafel plot analysis (Fig. 4b) provides further insights into the kinetics of the HER for the synthesized tungsten carbide samples. The Tafel slopes of TC-1 to TC-4 fall within a similar range of 56.7, 53.2, 52.5, and 56.4 mV/dec, respectively. These values are significantly larger than the Tafel slope of 29.53 mV/dec observed for the Pt/C, suggesting more sluggish kinetics at low current densities compared to Pt/C. Based on the Tafel plot data, the rate-determining step for the tungsten carbide samples is likely the Heyrovsky reaction (electrochemical desorption of H_2) at low current densities [27]. Furthermore, as shown in Fig. S7, the Tafel slopes of the tungsten carbide samples remain below 120 mV/dec across different current density ranges, indicating rapid kinetic processes even at high current densities. Notably, TC-3 exhibits higher rapid kinetics compared to TC-1, TC-2, and TC-4, which can be attributed to a lower reaction resistance of TC-3 compared to the other samples. Such a lower reaction resistance of TC-3 can be linked to the optimal compositions of WC and W_2C phases. It is worth noting that while metallic W is less electrocatalytically active than WC and W_2C, it can enhance HER performance by facilitating electron transfer [39]. It should be noted that the HER kinetics for all the tungsten carbide samples appear faster than that of Pt/C at current densities larger than 100 mA/cm^2, indicating the superior HER performance of FJH-fabricated tungsten carbide catalysts operating at high current densities.

The charge transfer resistances of the tungsten carbide samples, as illustrated in the Nyquist plot (Fig. 4c) measured at a potential of 250 mV vs. RHE, show a strong correlation with the trends observed in the Tafel plot. Notably, the TC-3 sample demonstrates a significantly lower charge transfer resistance of 4.89 Ω compared to the other electrocatalysts, highlighting its ability to facilitate more efficient electron transfer. This reduction in charge transfer resistance suggests that the phase ratio of WC to W_2C in TC-3 highly promotes the charge transfer and facilitates faster kinetics of HER in acidic media. The charge transfer resistance for the TC-3 sample, shown in Fig. 4d, decreases as the potential increases, suggesting improved kinetics and more efficient charge transfer at higher current densities. The comparable electrocatalytic performance of TC-2 and TC-3, despite their different WC:W_2C ratios (Fig. 2a), can be attributed to the combined influence of active site density, synergistic phase interactions, and particle morphology. Both WC and W_2C contribute to HER activity, with WC providing stability and W_2C enhancing conductivity. The synergistic effects between the two phases, along with similar active site density and microstructural properties (e.g., surface area and porosity) lead to the comparable performance of TC-2 and TC-3 catalysts.

To elucidate the electrochemical activity of the phase-engineered electrocatalysts, double-layer capacitance (C_{dl}) and ECSA were calculated as indicators of the electrocatalyst activity. C_{dl} was determined through cyclic voltammetry at different scan rates within the non-faradaic window (Figs. S8–S11). As illustrated in Fig. 4e, the TC-3 electrocatalyst exhibited the highest C_{dl} value of 77.84 mF/cm^2, followed by TC-2 (73.42 mF/cm^2), TC-4 (23.05 mF/cm^2), and TC-1 (19.47 mF/cm^2). Based on these C_{dl} values, the ECSA was calculated for each electrocatalyst: 1946 cm^2 for TC-3, 1835.50 cm^2 for TC-2, 576.25 cm^2 for TC-4, and 486.75 cm^2 for TC-1. These results clearly evidence the superior performance of TC-3 compared to the other electrocatalysts.

Long-term stability is a crucial performance indicator for HER catalysts, particularly in acidic environments. The durability of the optimized TC-3 catalyst was evaluated by conducting stability tests at a high current density of 4 A/cm^2. Remarkably, the TC-3 catalyst demonstrates exceptional stability, maintaining a constant potential over an extended period of continuous electrolysis exceeding 230 h (>9 days), as evident from Fig. 4f. The exceptional performance of TC-3 (e.g., long-term stability and low overpotential) at an ultrahigh current density of 4 A/cm^2 stands among the best electrocatalysts reported in prior work for acidic HER (Table S1) [40–43]. The hydrogen throughput of TC-3 samples is

displayed in comparison with those of state-of-the-art catalysts, as shown in Fig. S13, demonstrating the superiority of the fabricated TC-3 catalysts. The outstanding stability of the TC-3 catalyst can be attributed to the inherent corrosion resistance of tungsten carbides and the strong bonding between tungsten carbide and the substrate formed during the synthesis process.

After the stability test, the overpotential of the TC-3 sample increases by 60 mV at 4 A/cm^2, as shown in Fig. S14. To investigate the underlying mechanisms of performance degradation of TC-3 catalysts, characterizations such as XRD, SEM, and Raman spectroscopy were conducted on samples after long-term stability testing at high current densities. Comparative XRD patterns (Fig. S16) of TC-3 before and after the stability test demonstrate a significant reduction in the intensity of tungsten carbide phase peaks. This reduction indicates structural changes such as phase dissolution or surface reconstruction under electrochemical testing conditions. Raman spectra (Fig. S17) reveal a decrease in the intensity of the characteristic tungsten carbide peak at 686 cm^{-1} after the test, alongside the appearance of a new peak at ~940 cm^{-1}, which is attributed to the formation of tungsten oxide. These observations collectively suggest that surface reconstruction occurred, partially transforming tungsten carbide into a less crystalline or amorphous tungsten oxide layer during the prolonged HER operation at high current densities (i.e., 4 A/cm^{-2}). Additionally, SEM images (Fig. S18) exhibit more compact and aggregated nanoparticles after the long-term stability testing, indicating nanoparticle coalescence. The phenomenon is likely driven by the dynamic electrochemical environment, which may contribute to performance degradation of the catalysts.

To examine the underlying mechanism of HER enhancement by forming multiphase tungsten carbide electrocatalyst, density functional theory (DFT) calculation was conducted. WC, W_2C and multiphase WC/W_2C structures were modeled (Fig. 5a–c). WC was transformed from hexagonal to orthorhombic phase to construct the interface structure in the composite material. The multiphase tungsten carbides show fine atomic alignment at the interface between WC and W_2C, indicating structurally stable interface with comparable stability to WC or W_2C. In addition, electronic structures were also analyzed to confirm property modulation originating from composite material formation (Fig. 5d). Multiphase tungsten carbides exhibit a d-band center of W ranging from −3.72 eV to −4.22 eV, while WC and W_2C exhibit constant d-band centers of −3.79 eV and −4.06 eV. It is inferred that W elements of multiphase materials experience various property modulations from different bonding environments at the interface as shown in Fig. 5c. In particular, multiphase tungsten carbides possess W elements with lower d-band center than WC and W_2C, indicating some W elements in the multiphase tungsten carbides are more stabilized in the multiphase tungsten carbides. Then, the more stabilized W in the multiphase tungsten carbides would relatively weaken the bond with H, promoting hydrogen evolution more than pristine WC and W_2C. This theoretical analysis facilitates better understanding of the experiment results (Fig. 4a).

4. Conclusion

A facile and rapid FJH method has been successfully employed to synthesize tungsten carbide electrocatalysts with well-controlled phase compositions, demonstrating exceptional acidic HER catalytic activity, particularly at high current densities. The tungsten carbide electrocatalysts were synthesized with varying FJH durations to tailor the phase composition, enabling the coexistence of WC and W_2C phases and capitalizing on their potential synergistic effects. Notably, the TC-3 catalyst outperformed other tungsten carbide catalysts, with a low overpotential (387 mV) achieved at a high current density of 4 A/cm^2. Moreover, the TC-3 catalyst showcases its exceptional stability by maintaining a constant potential during continuous electrolysis for over 230 h (>9 days), which sets it among the best acidic HER electrocatalysts. This outstanding combination of high efficiency and exceptional stability renders the TC-3 catalyst a promising candidate for industrial-scale hydrogen production applications.

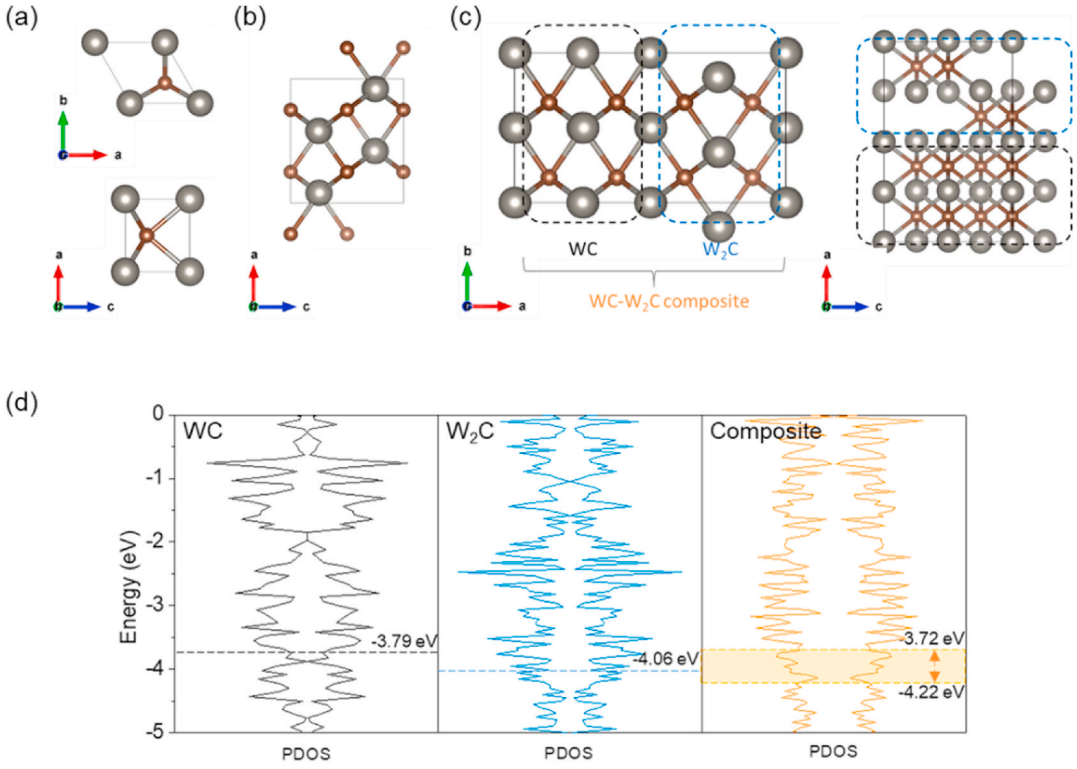

Fig. 5. Atomic structures of (a) WC, (b) W_2C and (c) WC-W_2C composite. (d) Projected density of states (PDOS) of W in WC, W_2C and multiphase tungsten carbides. (Dotted lines are d-band centers.)

CRediT authorship contribution statement

Amirarsalan Mashhadian: Writing – original draft, Visualization, Validation, Methodology, Investigation, Formal analysis, Data curation, Conceptualization. **Shiwen Wu:** Writing – review & editing, Investigation, Formal analysis. **Taesoon Hwang:** Investigation, Writing – original draft. **Yun Hao:** Investigation, Formal analysis. **Mahdi Mosadegh:** Validation, Investigation. **Kyeongjae Cho:** Writing – review & editing, Methodology, Conceptualization. **Dewen Hou:** Validation, Investigation. **Tianyi Li:** Writing – review & editing, Investigation, Funding acquisition. **Majid Minary-Jolandan:** Writing – review & editing, Supervision, Resources, Methodology. **Guoping Xiong:** Writing – review & editing, Supervision, Resources, Methodology, Funding acquisition, Conceptualization.

Declaration of competing interest

The authors declare that they have no known competing financial interests or personal relationships that could have appeared to influence the work reported in this paper.

Acknowledgment

G.X. thanks the University of Texas at Dallas startup fund. Work performed at the Center for Nanoscale Materials, a U.S. Department of Energy Office of Science User Facility, was supported by the U.S. DOE, Office of Basic Energy Sciences, under Contract No. DE-AC02-06CH11357.

Appendix A. Supplementary data

Supplementary data to this article can be found online at https://doi.org/10.1016/j.ijhydene.2025.01.487.

References

[1] Ellabban O, Abu-Rub H, Blaabjerg F. Renewable energy resources: current status, future prospects and their enabling technology. Renew Sustain Energy Rev 2014;39:748–64.
[2] Chu S, Majumdar A. Opportunities and challenges for a sustainable energy future. Nature 2012;488:294–303.
[3] Liu W, Liu Q, Wan X, Shui J. Boosting the oxygen reduction performance of Fe–N–C catalyst using zeolite as an oxygen reservoir. Trans Tianjin Univ 2024;30:428–35.
[4] Sazali N. Emerging technologies by hydrogen: a review. Int J Hydrogen Energy 2020;45:18753–71.
[5] Luo F, et al. Hydrazine-Assisted acidic water splitting driven by iridium single atoms. Adv Sci 2023;10:2305058.
[6] Xie Y, et al. Stable and high-performance Ir electrocatalyst with boosted utilization efficiency in acidic overall water splitting. Chem Eng J 2021;424:130337.
[7] Zhang Q, Wang B. Development and challenges of electrode ionomers used in the catalyst layer of proton-exchange membrane fuel cells: a review. Trans Tianjin Univ 2023;29:360–86.
[8] Lu JL, Li ZH, Jiang SP, Shen PK, Li L. Nanostructured tungsten carbide/carbon composites synthesized by a microwave heating method as supports of platinum catalysts for methanol oxidation. J Power Sources 2012;202:56–62.
[9] Guo L, et al. Robust hydrogen evolution reaction catalysis by ultrasmall amorphous ruthenium phosphide nanoparticles. Chem Commun 2019;55:7623–6.
[10] Zhang Q, et al. Constructing successive active sites for metal-free electrocatalyst with boosted electrocatalytic activities toward hydrogen evolution and oxygen reduction reactions. ChemCatChem 2018;10:5194–200.
[11] Shi J, et al. Enabling high-efficiency ethanol oxidation on NiFe-LDH via deprotonation promotion and absorption inhibition. J Energy Chem 2023;85:76–82.
[12] Zhou S, et al. Surface-growing organophosphorus layer on layered double hydroxides enables boosted and durable electrochemical freshwater/seawater oxidation. Appl Catal B Environ 2023;332:122749.
[13] Luo F, et al. Atomically dispersed Ni electrocatalyst for superior urea-assisted water splitting. J Energy Chem 2024;90:1–6.
[14] kong W, et al. Platinum nickel alloy-MXene catalyst with inverse opal structure for enhanced hydrogen evolution in both acidic and alkaline solutions. Nano Res 2023;16:195–201.
[15] Shah AH, Wan C, Huang Y, Duan X. Toward molecular level understandings of hydrogen evolution reaction on platinum surface. J Phys Chem C 2023;127:12841–8.
[16] Sun J, Ge Q, Guo L, Yang Z. Nitrogen doped carbon fibers derived from carbonization of electrospun polyacrylonitrile as efficient metal-free HER electrocatalyst. Int J Hydrogen Energy 2020;45:4035–42.
[17] Seh ZW, et al. Combining theory and experiment in electrocatalysis: insights into materials design. Science 2017;355:eaad4998.
[18] Liu D, et al. Multi-phase heterostructure of CoNiP/Co_xP for enhanced hydrogen evolution under alkaline and seawater conditions by promoting H_2O dissociation. Small 2021;17:2007557.
[19] Sheng W, et al. Correlating hydrogen oxidation and evolution activity on platinum at different pH with measured hydrogen binding energy. Nat Commun 2015;6:5848.
[20] Li J, et al. Stable NiPt–Mo2C active site pairs enable boosted water splitting and direct methanol fuel cell. Green Energy Environ 2023;8:559–66.
[21] Liu Z, et al. Pt/Mo_2C heteronanosheets for superior hydrogen evolution reaction. J Energy Chem 2020;47:317–23.
[22] Jun H, Kim S, Lee J. Development strategies in transition metal carbide for hydrogen evolution reaction: a review. Kor J Chem Eng 2020;37:1317–30.
[23] Huang J, Hong W, Li J, Wang B, Liu W. High-performance tungsten carbide electrocatalysts for the hydrogen evolution reaction. Sustain Energy Fuels 2020;4:1078–83.
[24] Harnisch F, Sievers G, Schröder U. Tungsten carbide as electrocatalyst for the hydrogen evolution reaction in pH neutral electrolyte solutions. Appl Catal B Environ 2009;89:455–8.
[25] Ngo Y-LT, et al. Carbide-directed enhancement of electrochemical hydrogen evolution reaction on tungsten carbide–oxide heterostructure. Chem Eng J 2022;450:137915.
[26] Zhang X, et al. Encapsulating dual-phased Mo2C-WC nanocrystals into ultrathin carbon nanosheet assemblies for efficient electrocatalytic hydrogen evolution. Chem Eng J 2021;408:127270.
[27] Li C, et al. Ultrafast self-heating synthesis of robust heterogeneous nanocarbides for high current density hydrogen evolution reaction. Nat Commun 2022;13:3338.
[28] Riedmayer R, Paren BA, Schofield L, Shao-Horn Y, Mallapragada D. Proton exchange membrane electrolysis performance targets for achieving 2050 expansion goals constrained by iridium supply. Energy Fuels 2023;37:8614–23.
[29] Huang A, et al. Mo_2C-Based ceramic electrode with high stability and catalytic activity for hydrogen evolution reaction at high current density. Small 2024;20:2308068.
[30] Zan L, et al. Investigation of the synergistic effect on cobalt oxide modified silver surface for electrocatalytic hydrogen evolution reaction. J Alloys Compd 2021;869:159324.
[31] Perdew JP, Burke K, Ernzerhof M. Generalized gradient approximation made simple. Phys Rev Lett 1996;77:3865–8.
[32] Emin S, et al. Tungsten carbide electrocatalysts prepared from metallic tungsten nanoparticles for efficient hydrogen evolution. Appl Catal B Environ 2018;236:147–53.
[33] Ling Y, et al. Construction of Mo_2C/W_2C heterogeneous electrocatalyst for efficient hydrogen evolution reaction. Int J Hydrogen Energy 2021;46:9699–706.
[34] Meng S, et al. Synthesis and characterization of molybdenum carbide catalysts on different carbon supports. Catal Today 2022;402:266–75.
[35] Chen Z, et al. Eutectoid-structured WC/W_2C heterostructures: a new platform for long-term alkaline hydrogen evolution reaction at low overpotentials. Nano Energy 2020;68:104335.
[36] Kornaus K, Gubernat A, Zientara D, Rutkowski P, Stobierski L. Mechanical and thermal properties of tungsten carbide – graphite nanoparticles nanocomposites. Pol J Chem Technol 2016;18:84–8.
[37] Tallo I, Thomberg T, Kontturi K, Jänes A, Lust E. Nanostructured carbide-derived carbon synthesized by chlorination of tungsten carbide. Carbon N. Y. 2011;49:4427–33.
[38] Fan X, et al. Synergistic effect of dual active sites over Ru/α-MoC for accelerating alkaline hydrogen evolution reaction. Appl Catal B Environ 2022;318:121867.
[39] Hu Y, et al. Scalable synthesis of heterogeneous W–W_2C nanoparticle-embedded CNT networks for boosted hydrogen evolution reaction in both acidic and alkaline media. ACS Sustainable Chem Eng 2019;7:10016–24.
[40] Liu R, et al. Design of aligned porous carbon films with single-atom Co–N–C sites for high-current-density hydrogen generation. Adv Mater 2021;33:2103533.
[41] Chen Y, et al. Highly active, nonprecious electrocatalyst comprising borophene subunits for the hydrogen evolution reaction. J Am Chem Soc 2017;139:12370–3.
[42] Zheng Z, et al. Boosting hydrogen evolution on MoS_2 via co-confining selenium in surface and cobalt in inner layer. Nat Commun 2020;11:3315.
[43] Mishra IK, et al. Hierarchical CoP/Ni_5P_4/CoP microsheet arrays as a robust pH-universal electrocatalyst for efficient hydrogen generation. Energy Environ Sci 2018;11:2246–52.